Nanoscale

RSC Publishing

COMMUNICATION

Rough contact is not always bad for interfacial energy coupling

Cite this: *Nanoscale*, 2013, **5**, 11598

Jingchao Zhang,[a] Yongchun Wang[b] and Xinwei Wang*[ab]

Received 28th July 2013
Accepted 23rd September 2013

DOI: 10.1039/c3nr03913g

www.rsc.org/nanoscale

For the first time we report that by introducing sub-nm roughness on a Si surface, the energy coupling between a single layer graphene (SLG) and the Si substrate can be improved substantially. This is contrary to the traditional view that a rough surface contact will weaken the energy coupling, rather than improve it. Periodical grooves of 2 nm width and 2 nm spacing are introduced on the surface of a Si substrate. It is surprisingly found that when the groove depth (δ) is less than 0.54 nm, the interfacial thermal resistance decreases against the increasing δ (more than 10% decrease at δ = 0.54 nm). The observed finding is explained soundly with the interfacial C–Si bond tuning by the surface roughness. For δ < 0.54 nm, the C–Si bond length in the suspended graphene region is large, and graphene experiences a strong pulling-down force (attractive) from the Si substrate. On the other hand, the graphene in the supported region is in direct contact with Si and experiences an extremely strong repulsive force to balance the pulling-down force in the suspended region. The repulsive force on graphene in the supported region can reach a level of 228 MPa. This significantly increases the local energy coupling and offsets the energy coupling reduction in the suspended graphene region. The discovery in this work points out that for extremely soft materials like graphene, it is possible to tune the material–substrate bonding by introducing sub-nm roughness on the substrate surface to significantly improve interfacial energy coupling.

Owing to its excellent thermal and electronic properties, graphene demonstrates great potential for practical applications in microelectronics and thermal management structures.[1–4] Recent experimental studies measured the thermal conductivity of graphene at around 3000–5000 W m^{-1} K^{-1}, depending on the graphene flake size and temperature.[3,4] Other groups using first principle calculations found the thermal conductivity of graphene in the range of 2000–6000 W m^{-1} K^{-1}.[5,6] The in-plane thermal conductivity of graphene decreases significantly when it is in contact with a substrate or for confined graphene nanoribbons (GNRs).[1,7–10] Due to damping of the flexural acoustic (ZA) phonons, the coupling to the substrate reduces the thermal conductivity of supported graphene by an order of magnitude.[11] To address the thermal transport in supported graphene, Seol *et al.*[12] carried out full quantum mechanical calculations of both normal and umklapp three-phonon scattering processes. They proved that the thermal conductivity of supported graphene is suppressed due to ZA phonon leakage across the graphene–substrate interface. Chen *et al.*[13] conducted spectral energy density (SED) analysis for phonons in supported graphene and found that the ZA phonon shifts to higher frequencies and the zone-center peak is notably broadened compared to suspended cases. This suggests that ZA phonons are greatly suppressed by the graphene–substrate interactions in supported graphene.

The limited internal phonon coupling and transfer within graphene in the out-of-plane direction significantly affects graphene–substrate interfacial phonon coupling and scattering, and leads to unique interfacial thermal transport phenomena. A very high interfacial thermal resistance of $5.30^{+0.46}_{-0.46} \times 10^{-5}$ K m^2 W^{-1} is observed by using the Raman frequency method under surface Joule heating.[14] The thermal contact resistance between graphene and SiO_2 was measured at 5.6×10^{-9}–1.2×10^{-8} K m^2 W^{-1} using a differential 3ω method.[15] Using nonequilibrium molecular dynamics (NEMD) simulation, Wei *et al.*[16] calculated the interfacial thermal resistance between two neighboring graphene layers at $\sim 4 \times 10^{-9}$ K m^2 W^{-1}. Understanding and control of the interfacial thermal resistance is crucial to the development of high performance graphene-based devices.[17] The thermal resistance is a major limiting factor for the related nanoscale thermal engineering.

In this work, the thermal transport across the interface of graphene and the silicon substrate is explored by performing MD simulations. The dynamic response of graphene to a

[a]*Department of Mechanical Engineering, 2010 Black Engineering Building, Iowa State University, Ames, IA 50011, USA. E-mail: xwang3@iastate.edu; Fax: +1-515-294-3261; Tel: +1-515-294-2085*

[b]*School of Environmental and Municipal Engineering, Qingdao Technological University, Qingdao, Shandong, 266033, P.R. China*

thermal impulse is investigated and the interfacial thermal resistance between graphene and Si is evaluated. Nanoscale roughness is introduced on the Si surface to tune the Si–C interaction and energy coupling. A transient pump-probe method is designed for interfacial thermal resistance characterization. Compared to the traditional NEMD method, this pump-probe technique is focused on the dynamic thermal response of the system and can greatly reduce the computation time. Energy evolution in transient simulation is tracked and discussed for the supported graphene. The silicon substrate is chosen because of its broad applications in nanoelectronics.[18–21]

Fig. 1(a) shows the physical domain construction for a single-layer graphene on a Si substrate. The second generation of the Brenner potential,[22] reactive empirical bond-order (REBO), based on the Tersoff potential[23,24] with interactions between C–C bonds is employed to model the graphene system. The Tersoff potential[23,24] with interactions between Si–Si bonds is used to model the silicon system. The REBO potential is chosen because its functions and parameters are known to give reasonable predictions for the thermal properties of graphene,[14] whereas the adaptive intermolecular reactive empirical bond-order (AIREBO) was reported to underestimate the dispersion of ZA phonons in graphene.[25] It has been proposed that the interactions between carbon atoms and the substrate are primarily short-range van der Waals type (vdW).[26,27] Therefore, the C–Si couplings are modeled as vdW interactions using the Lennard-Jones (LJ) potential $V(r) = 4\varepsilon[(\sigma/r)^{12} - (\sigma/r)^{6}]$, where σ is the distance parameter, ε is the energy parameter and r is the interatomic distance. The ε parameter determines the strength of the specific interactions between graphene and silicon. In this work, ε and σ are set as 8.909 meV and 3.326 Å respectively.[28] In experimental studies, the bond type between interfaces will depend on the graphene synthesis and sample preparation procedures. For epitaxial graphene samples grown on a substrate, the bond type will be covalent. If the graphene is produced by mechanical exfoliation[29,30] or chemical vapor deposition (CVD)[31,32] and then transplanted to the experiment substrate,[33] the interfacial interactions will most likely be vdW. For industrial applications, the grooved silicon substrate and monolayer graphene in nano-devices are expected to be prepared separately and then combined together. Therefore it is reasonable to use the LJ potential in this study. Also, due to the intrinsic corrugation nature of graphene,[34,35] loose contacts between graphene and the substrate will exist in most cases, which can only be described by the long range vdW forces. To save computational time, the LJ potential is truncated at the cut-off distance of $r_c = 3.5\sigma$. The initial atomic velocities in each direction are extracted from the Gaussian distribution for the given temperature 300 K. At the start of simulation, the position of the GNR is located 3.7 Å above the upper layer of the Si bulk. Periodic boundary conditions are applied to the x and y directions and free boundary conditions to the z direction. Dimensions of the GNR are smaller than those of the silicon to avoid boundary interactions through the periodic boundaries. The step for time integration is 0.5 fs (1 fs = 10^{-15} s). All MD simulations are performed using the large-scale atomic/molecular massively parallel simulator (LAMMPS) package.[36]

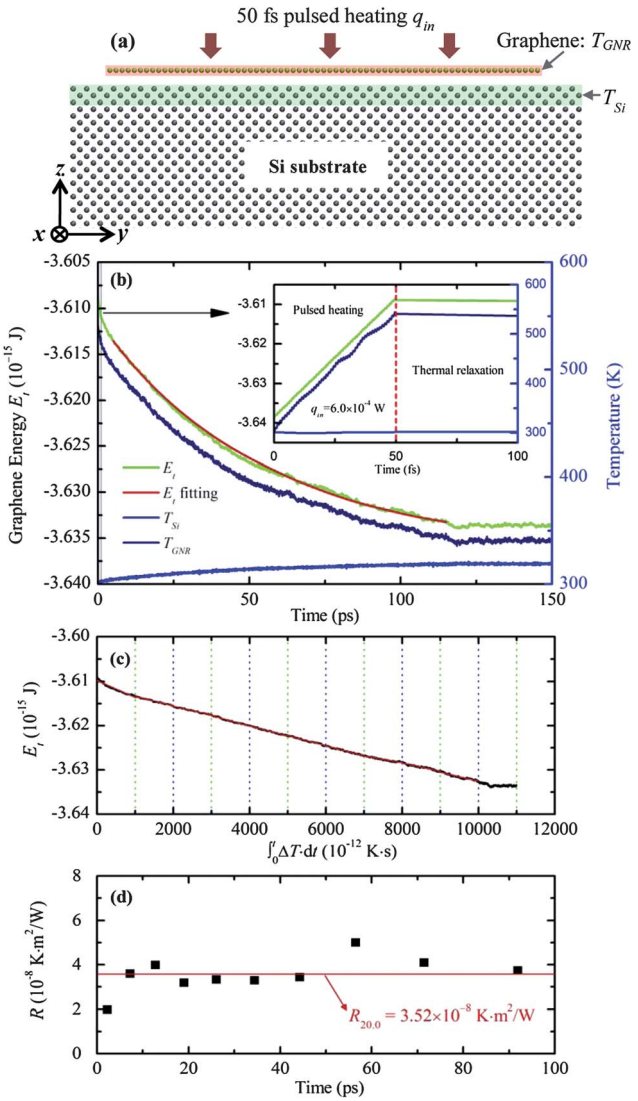

Fig. 1 (a) Atomic configuration of the GNR and silicon system. Periodic boundary conditions are applied to the x and y directions and free boundary conditions to the z direction. A thermal impulse $\dot{q}_{in}$ is imposed on the supported GNR after thermal equilibrium calculation and the top three layers of silicon atoms are grouped to calculate the surface temperature of the silicon substrate. (b) Temperature evolutions (right y axis) of the 4.1 × 18.3 nm^2 (x × y) GNR and Si for the first 50 fs pulsed thermal excitation and following 150 ps thermal relaxation. The overall GNR energy (E_t) and fitting results are shown in the figure (left y axis). The calculated interface thermal resistance from this overall fitting method is 3.52 × 10^{-8} K m^2 W^{-1}. The fitting profile calculated from a single R value soundly matches the MD simulation result. (c) By integrating the temperature differences between T_{GNR} and T_{Si}, the energy relaxation profile of GNR can be correlated to $\Delta T dt$ directly. (d) Slope of the profile in (c) can be linearly fitted to calculate the segment interfacial thermal resistance values, which is around the overall fitting results.

The pump-probe transient thermoreflectance method has been widely used to study the thermal transport in bulk materials and thin films.[37] The Kapitza resistance and heat flow across material interfaces can be measured using this optical technique.[38] In this work, a pump-probe method is developed using MD simulation to calculate the interfacial thermal resistance between graphene nanoribbons and silicon crystal. As shown in Fig. 1(b), after the MD system reaches thermal

equilibrium, an ultrafast heat impulse is imposed on the supported GNR. In the heating process, non-translational kinetic energy is evenly added to the GNR system in each direction by rescaling velocities of atoms. When the excitation is released, the temperature of the GNR (T_{GNR}) increases dramatically and then gradually reduces during the thermal relaxation process. In our work, three layers of silicon atoms beneath the supported GNR are grouped to calculate the surface temperature of the silicon bulk (T_{Si}) as shown in Fig. 1(a). T_{GNR}, T_{Si} and GNR system energy (E_t) are recorded each time step during the thermal relaxation. In the MD simulation, the energy decay of the GNR is only caused by its thermal energy loss to the silicon system. Therefore, given the energy and temperature evolution of the graphene system, the interfacial thermal resistance (R) between the supported GNR and silicon substrate can be calculated using the equation

$$\frac{\partial E_t}{\partial t} = \frac{T_{GNR} - T_{Si}}{R/A}, \quad (1)$$

where E_t is the system energy of the supported GNR and A is GNR's area. An instant R can be calculated at each time step according to the local energy changing rate and corresponding temperature difference. We have tried this method and found it subject to the noise in the energy decay and the calculated interface thermal resistance has very large uncertainty. If R has little variation within the temperature range during thermal relaxation, a constant R value can be substituted in eqn (1) to predict the E_t profile. Under such a scenario, the interfacial thermal resistance can be calculated by best fitting of the E_t profile using the least square method using an integral form of eqn (1) as detailed below.

To understand the thermal transport across graphene and the substrate interface, a silicon crystal with dimensions of $5.8 \times 20.0 \times 5.4$ nm^3 ($x \times y \times z$) is built. The size of the supported GNR is 4.1×18.3 nm^2 ($x \times y$). After 300 ps canonical ensemble (NVT) and 100 ps microcanonical ensemble (NVE) calculation, the whole system reaches thermal equilibrium at 300 K. We have also run long-time calculations with NVE for 1.5 ns. It is observed that the surface structure has a good stability, and the above 300 ps NVE calculation indeed gives a stable structure similar to that given by the long-time calculations. Then the GNR is exposed to a thermal impulse of $\dot{q}_{in} = 6.0 \times 10^{-4}$ W for 50 fs. After the excitation, T_{GNR} increases to 535.3 K and the adjacent silicon surface temperature T_{Si} is 301.5 K as shown in Fig. 1(b). In the following 150 ps thermal relaxation process, energy dissipation from graphene to the silicon substrate is recorded and the interfacial thermal resistance is calculated. The equilibrium distance between graphene and the Si-substrate surface is 3.2 Å based on the modeling. Energy and temperature results are averaged by 100 in the calculation to suppress data noise. Temperature evolutions and energy fitting results are shown in Fig. 1(b). It is observed that after the 50 fs thermal excitation is released, the energy of the graphene goes down quickly due to the energy transfer to the Si-substrate. At the same time, the graphene temperature also goes down accordingly and a slight temperature rise is observed for the silicon atoms adjacent to the interface. The energy decay fitting in Fig. 1(b) is performed based on eqn (1) and takes the integral form of $E_t = E_0 + (R/A)\int_0^t (T_{GNR} - T_{Si})dt$. Here R is treated as a constant, and such assumption will be discussed and validated later. E_0 is graphene's initial energy.

The calculated thermal resistance $R_{20.0}$ is 3.52×10^{-8} K m^2 W^{-1}, which is in the same magnitude with previous studies of graphene on 6H–SiC and SiO_2.[15,39] As shown in Fig. 1(b), the energy decay curve and temperature decay curve for the GNR are parallel to each other. In fact, a fitting can also be applied to the temperature decay curve of GNR to determine the interface thermal resistance. Such a process will need knowledge of the specific heat of GNR, so we prefer to use the energy decay of GNR directly. At the beginning of the thermal relaxation process, a faster decay in GNR's total energy is observed. This is caused by the strong energy disturbance induced by the thermal impulse to the system. During that period, the potential and kinetic energies have not yet reached equilibrium. Therefore, the initial part (5 ps) of the thermal relaxation profile is strongly dominated by the energy transfer from kinetic to potential energy in graphene, and is excluded from our fitting process. It can be observed from Fig. 1(b) that the fitting curve soundly matches the energy profile using a constant $R_{20.0}$. This leads to a strong point that the interfacial thermal resistance between GNR and Si does not have large change over the relaxation temperature 300 K–500 K. As the energy decay is driven by the temperature difference $\Delta T = T_{GNR} - T_{Si}$, in Fig. 1(c), we plot out how the graphene energy changes against $\int_0^t \Delta T dt$. It is observed that the E_t profile has a linear relationship with $\int_0^t \Delta T dt$, which further proves the fact that the thermal resistance R is nearly constant during the relaxation process. In fact, we can use this profile to determine the interfacial thermal resistance. The E_t profile is divided into many segments as shown in Fig. 1(c). For each segment (t_1 to t_2), R can be treated constant, and can be determined by linear fitting of the curve in Fig. 1(c). The fitted slope equals A/R, and can be used to determine R. The calculated results are shown in Fig. 1(d). It is observed that instant R values vary around the overall fitting results $R_{20.0}$. Therefore it is conclusive that the thermal resistance is constant and has weak dependence on the GNR and Si temperatures.

In the above calculations, T_{GNR} is higher than T_{Si} during the thermal relaxation process. To address the thermal rectification across GNR and substrate interfaces, cases with $T_{GNR} < T_{Si}$ are investigated and the calculated thermal resistance results have little difference from that with $T_{GNR} > T_{Si}$. This demonstrates that there is no thermal rectification during the thermal transport across the graphene–Si interface. The confined dimension in the lateral directions of supported graphene will greatly affect the phonon behavior at the graphene–substrate interface. Therefore, it is of great interest to investigate the effects of dimension on the interfacial thermal resistance between graphene and silicon. For this purpose, the width of the supported GNR is fixed at 4.1 nm and lengths of 1.6, 2.7, 8.6, 18.3, 38.5 and 78.2 nm cases are calculated. It is found that

the calculated thermal resistance increases at small GNR length and converges at large length scales. The physical mechanism for this phenomenon lies in the differences between the actual heat transfer area (A_a) on the Si-substrate and the projected area (A_p) of graphene used in the fitting method. Since the cut-off distance (11.641 Å) between GNR and the Si-substrate is larger than their equilibrium distance (3.2 Å), A_a is larger than A_p. This area difference cannot be neglected at small systems and leads to thermal resistance increase with the graphene size at small scales. The study of this work is focused on the 4.1×18.3 nm^2 ($x \times y$) case.

Graphene is considered a promising nanomaterial with applications in nanoelectronics and nanocircuits. Our previous research has revealed that when graphene nanoribbons are bent to fit the substrate structure, a thermal resistance will emerge in the bending area due to local phonon reflection and scattering.[40] Aside from bent structures in applications, the substrate surfaces are often dented with patterns to achieve maximum thermal radiation and realize various electrical functions. In spite of the vast applications of graphene in nanoelectronics, however, to the best of our knowledge, the effects of surface roughness on the thermal transport across graphene–substrate interface have not been studied. In the below section, the interfacial thermal resistance between graphene and the rough silicon substrate of well-defined roughness is studied.

During our rough surface effect study, a silicon substrate with a dimension of $5.8 \times 20.0 \times 5.4$ nm^3 ($x \times y \times z$) is built and the size of the supported GNR is 4.1×18.3 nm^2 ($x \times y$). The physical domain construction follows that shown in Fig. 1(a). There could be millions of roughness patterns on the surface of the Si-substrate and it is impossible to calculate all of them. To simplify this study, only one of the patterns is used in this work and variations are made by changing the groove depth δ. In our pattern and system design, grooves are made in the x direction of the Si-substrate and the width for each groove is ~2.0 nm, which is the same as the separation distance for the neighboring grooves. Atomic configurations of the systems after thermal equilibrium are shown in Fig. 2(a)–(c) and the insets of Fig. 2(d). Periodic boundary conditions are applied to the x and y directions and free boundary conditions are applied to the z direction. It is observed that when $\delta = 0.54$ nm, the graphene is bent to fit the Si-substrate surface and both the supported and suspended areas are in close contact with Si. For $\delta = 0.68$ nm, most of suspended graphene areas remain in close contact with the Si-substrate but are partially separated from Si. While for the $\delta = 0.81$ nm case, all the suspended areas of the graphene are separated from the Si-substrate. The reasons for such differences will be elucidated in the following discussions. Take the $\delta = 2.0$ nm case as an example, after 300 ps NVT and 100 ps NVE calculations, the whole system reaches a thermal equilibrium at 300 K. Then a thermal impulse of $\dot{q}_{in} = 6.0 \times 10^{-4}$ W is applied to the supported GNR for 50 fs. The whole system is then left for thermal relaxation under NVE calculation for another 150 ps. The calculated thermal resistance ($R_{\delta=2.0\ nm}$) is 4.42×10^{-8} K m^2 W^{-1}, 26% larger than the flat surface case under the same conditions.

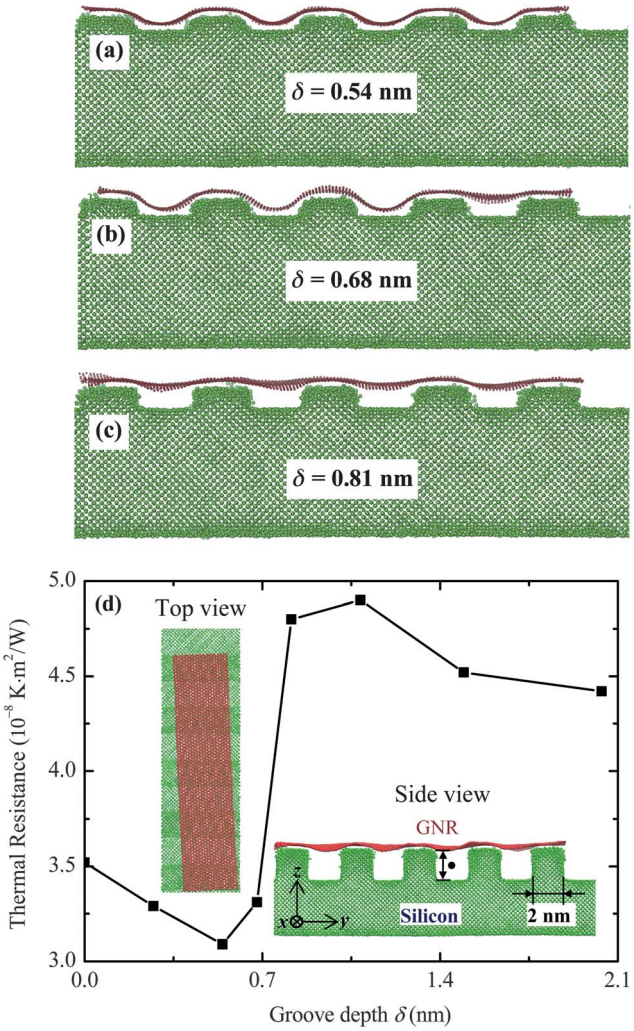

Fig. 2 (a)–(c) Atomic configurations for $\delta = 0.54$, $\delta = 0.68$ and $\delta = 0.81$ nm cases. (d) Interfacial thermal resistance variation against surface roughness/groove depth. Top and side views of the $\delta = 2.0$ nm case are depicted in the insets.

To investigate the interfacial thermal resistance relationship with surface roughness, variations have been made on the groove depth δ and cases of $\delta = 0.27$, 0.54, 0.68, 0.81, 1.09, 1.49, and 2.0 nm are studied. Groove depths larger than 2.0 nm are not studied because the cut-off distance for the 12-6 LJ potential is only 1.16 nm. Therefore it is safe to speculate that the thermal resistance values will not change substantially for $\delta > 2.0$ nm. The calculated thermal resistance is shown in Fig. 2(d) against the groove depth. For the results in Fig. 2(d), the real areas of the graphene, not their projected areas on the Si substrate, are used for resistance evaluation. It is very surprising and interesting to observe that the interfacial thermal resistance first decreases as δ becomes larger when the groove depth is smaller than 7 Å. R reaches the lowest value of 3.09×10^{-8} K m^2 W^{-1} when δ is 5.4 Å. This is contrary to the traditional view that, in comparison with a flat surface, a rough surface should always give a larger interfacial thermal resistance due to the poor contact. To explain this new finding, the interatomic forces between graphene and silicon are calculated for the $\delta = 0.54$ nm case and

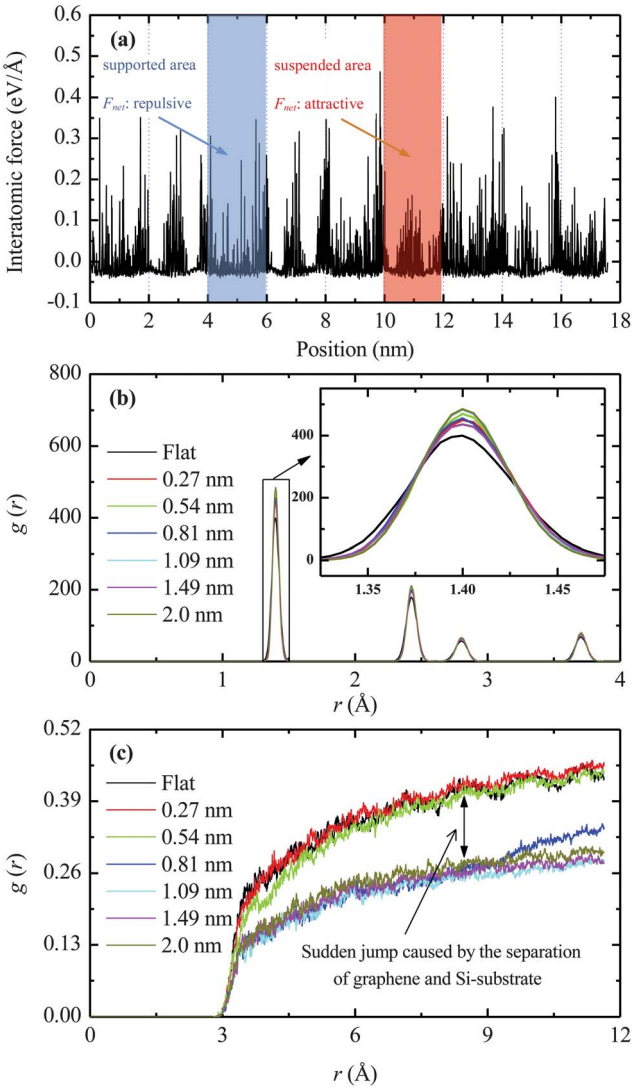

Fig. 3 (a) Interatomic forces between supported GNR and $\delta = 0.54$ nm dented silicon substrate. The blue and red shaded areas indicate the supported and suspended GNR regions respectively. (b) Radial distribution functions for the supported GNRs. The peaks are sharper for the dented Si cases, indicating stretching in graphene. (c) Radial distribution functions between graphene and the Si-substrate. The $g(r)$ values drop to significant lower levels when the groove depth δ becomes larger than 0.81 nm. This explains the sudden thermal resistance increase from $\delta = 0.51$ nm to $\delta = 0.81$ nm observed in Fig. 2(d).

the results are shown in Fig. 3(a). The supported and suspended areas are cross-adjacent and each region has a width of 2.0 nm. Due to the roughness of the silicon surface, the interatomic forces are not evenly distributed in the supported graphene. For graphene over the groove, most of the C–Si distance is large, beyond the repulsive force range. So the C–Si interaction is attractive. When the groove depth is small, this attractive force is strong enough to bend the graphene to fit the silicon surface. Since the overall force on the graphene will be zero on average, a net repulsive force will arise for the supported graphene areas. For example, at the location 4–6 nm in the length direction of the GNR [shown in Fig. 3(a)] the graphene is supported and the net interatomic force is calculated at +1.17 eV Å^{-1}. The positive sign indicates a repulsive force. This force gives a pressure of 228 MPa for the supported graphene. Such very high pressure will significantly reduce the local interfacial thermal resistance. At the location of 10–12 nm shown in Fig. 3(a), the graphene is suspended. The net force is −2.36 eV Å^{-1} and the negative sign indicates an attractive force. The contact pressure between the graphene and the Si-substrate increases greatly in the supported graphene region due to the significant attractive force in the suspended regions. This is like the supported graphene region is pulled down on both sides by the attractive force in the suspended regions. The significantly increased contact pressure in the supported graphene region leads to a decreased thermal resistance between graphene and silicon. This thermal resistance decrease offsets the thermal resistance increase in the suspended region, giving an overall thermal resistance decrease.

From the above discussion, it is realized that the graphene is kind of stretched by the attractive force in the suspended region and repulsive force in the supported region. Such stretching could be reflected by the structure of the graphene. The radial distribution function (RDF) of the GNRs is calculated and the results are shown in Fig. 3(b). Since all the GNRs share the same structure, their RDFs give the same formation for all cases. However, detailed inspections reveal that the peaks become narrower and sharper when GNRs are supported on the dented Si-substrate with a larger groove depth. Also a slight shift of the first peak location to a larger atomic-separation is observed. This firmly confirms that the structures of the GNRs on the dented Si surface are stretched due to the existence of grooves. For more relaxed GNRs, like that on the flat Si surface, the structure is more relaxed, and the RDF peak has a broader line width.

When δ becomes large enough, in the suspended region, a lot of graphene atoms will have very weak or zero interaction with Si atoms. To elucidate this phenomenon, the RDF between graphene and silicon are calculated and the results are shown in Fig. 3(c). It is observed that the $g(r)$ values are evidently larger at small groove depths and drop to a much lower level when δ is increased from 0.54 nm to 0.81 nm. This is corresponding to the jump of the interfacial thermal resistance from $\delta = 0.54$ nm to $\delta = 0.81$ nm observed in Fig. 2(d). This again proves the fact that when the groove depth is small, the supported graphene will stay close to the dented Si surface. When graphene in the suspended region is completely separated from Si (weak/no coupling), the thermal resistance jumps suddenly. At the same time, the repulsive force in the supported area becomes smaller, and the local thermal resistance increases due to the reduced localized pressure. Therefore the graphene hangs over the grooves and the corresponding thermal resistance increases due to significant reduction in the thermal contact area. In addition to the groove depth explored in this work, the interfacial thermal resistance is also dependent on many other characteristics of surface patterns, like surface orientation, details of atomic configuration, graphene–substrate contact area size and shape. Extensive studies are necessary in the near future to study their effects and optimize the surface nanoscale pattern to significantly improve interface energy coupling.

To sum up, this work investigated the thermal transport across the graphene–silicon interface using MD simulation. It was proved that the interfacial thermal resistance between graphene–Si is temperature independent (300–550 K) and there is no thermal rectification across the interface. The most significant discovery of this work is that a rough surface contact is not always bad for energy coupling. The interfacial thermal resistance can be reduced by tuning the depth of the groove. The interatomic forces between graphene–Si atoms increase the contact pressure for small groove depth ($\delta < 0.7$ nm) and this effect offsets the energy coupling reduction in the suspended graphene region, leading to an overall thermal resistance reduction and improved energy coupling. Our work provides a fundamental understanding of sub-nm rough surface interfacial thermal transport and can be used to improve the nano-device performance in thermal engineering with optimized nanoscale rough contact.

The support of this work from the National Science Foundation (CBET-1235852) is gratefully acknowledged. X.W. thanks the partial support of the "Taishan Scholar" program of Shandong Province, China.

References

1 W. W. Cai, A. L. Moore, Y. W. Zhu, X. S. Li, S. S. Chen, L. Shi and R. S. Ruoff, *Nano Lett.*, 2010, **10**, 1645–1651.
2 K. M. F. Shahil and A. A. Balandin, *Nano Lett.*, 2012, **12**, 861–867.
3 A. A. Balandin, *Nat. Mater.*, 2011, **10**, 569–581.
4 S. Ghosh, I. Calizo, D. Teweldebrhan, E. P. Pokatilov, D. L. Nika, A. A. Balandin, W. Bao, F. Miao and C. N. Lau, *Appl. Phys. Lett.*, 2008, **92**, 151911.
5 B. D. Kong, S. Paul, M. B. Nardelli and K. W. Kim, *Phys. Rev. B: Condens. Matter Mater. Phys.*, 2009, **80**, 033406.
6 D. L. Nika, S. Ghosh, E. P. Pokatilov and A. A. Balandin, *Appl. Phys. Lett.*, 2009, **94**, 203103.
7 E. Pop, V. Varshney and A. K. Roy, *Mrs Bull.*, 2012, **37**, 1273–1281.
8 Z. Q. Wang, R. G. Xie, C. T. Bui, D. Liu, X. X. Ni, B. W. Li and J. T. L. Thong, *Nano Lett.*, 2011, **11**, 113–118.
9 J. C. Zhang, X. P. Huang, Y. N. Yue, J. M. Wang and X. W. Wang, *Phys. Rev. B: Condens. Matter Mater. Phys.*, 2011, **84**, 235416.
10 L. Lindsay, D. A. Broido and N. Mingo, *Phys. Rev. B: Condens. Matter Mater. Phys.*, 2010, **82**, 115427.
11 Z. Y. Ong and E. Pop, *Phys. Rev. B: Condens. Matter Mater. Phys.*, 2011, **84**, 075471.
12 J. H. Seol, I. Jo, A. L. Moore, L. Lindsay, Z. H. Aitken, M. T. Pettes, X. S. Li, Z. Yao, R. Huang, D. Broido, N. Mingo, R. S. Ruoff and L. Shi, *Science*, 2010, **328**, 213–216.
13 J. Chen, G. Zhang and B. W. Li, *Nanoscale*, 2013, **5**, 532–536.
14 Y. N. Yue, J. C. Zhang and X. W. Wang, *Small*, 2011, **7**, 3324–3333.
15 Z. Chen, W. Jang, W. Bao, C. N. Lau and C. Dames, *Appl. Phys. Lett.*, 2009, **95**, 161910.
16 Z. Y. Wei, Z. H. Ni, K. D. Bi, M. H. Chen and Y. F. Chen, *Phys. Lett. A*, 2011, **375**, 1195–1199.
17 A. Venugopal, L. Colombo and E. M. Vogel, *Appl. Phys. Lett.*, 2010, **96**, 013512.
18 M. Halbwax, T. Sarnet, P. Delaporte, A. Sentis, H. Etienne, F. Torregrosa, V. Vervisch, I. Perichaud and S. Martinuzzi, *Thin Solid Films*, 2008, **516**, 6791–6795.
19 R. I. Bahar, D. Hammerstrom, J. Harlow, W. H. Joyner, C. Lau, D. Marculescu, A. Orailoglu and M. Pedram, *Computer*, 2007, **40**, 25–33.
20 C. M. Hu, *Nanotechnology*, 1999, **10**, 113–116.
21 L. A. Jauregui, Y. N. Yue, A. N. Sidorov, J. N. Hu, Q. K. Yu, G. Lopez, R. Jalilian, D. K. Benjamin, D. A. Delk, W. Wu, Z. H. Liu, X. W. Wang, Z. G. Jiang, X. L. Ruan, J. M. Bao, S. S. Pei and Y. P. Chen, *ECS Trans.*, 2010, **28**, 73–83.
22 D. W. Brenner, O. A. Shenderova, J. A. Harrison, S. J. Stuart, B. Ni and S. B. Sinnott, *J. Phys.: Condens. Matter*, 2002, **14**, 783–802.
23 J. Tersoff, *Phys. Rev. Lett.*, 1988, **61**, 2879–2882.
24 B. W. Dodson, *Phys. Rev. B: Condens. Matter Mater. Phys.*, 1987, **35**, 2795–2798.
25 L. Lindsay and D. A. Broido, *Phys. Rev. B: Condens. Matter Mater. Phys.*, 2010, **81**, 209903.
26 T. Hertel, R. E. Walkup and P. Avouris, *Phys. Rev. B: Condens. Matter Mater. Phys.*, 1998, **58**, 13870–13873.
27 J. L. Xiao, S. Dunham, P. Liu, Y. W. Zhang, C. Kocabas, L. Moh, Y. G. Huang, K. C. Hwang, C. Lu, W. Huang and J. A. Rogers, *Nano Lett.*, 2009, **9**, 4311–4319.
28 Z. Y. Ong and E. Pop, *Phys. Rev. B: Condens. Matter Mater. Phys.*, 2010, **81**, 155408.
29 Y. B. Zhang, Y. W. Tan, H. L. Stormer and P. Kim, *Nature*, 2005, **438**, 201–204.
30 K. S. Novoselov, A. K. Geim, S. V. Morozov, D. Jiang, M. I. Katsnelson, I. V. Grigorieva, S. V. Dubonos and A. A. Firsov, *Nature*, 2005, **438**, 197–200.
31 C. Mattevi, H. Kim and M. Chhowalla, *J. Mater. Chem.*, 2011, **21**, 3324–3334.
32 J. K. Wassei, M. Mecklenburg, J. A. Torres, J. D. Fowler, B. C. Regan, R. B. Kaner and B. H. Weiller, *Small*, 2012, **8**, 1415–1422.
33 J. W. Suk, A. Kitt, C. W. Magnuson, Y. F. Hao, S. Ahmed, J. H. An, A. K. Swan, B. B. Goldberg and R. S. Ruoff, *ACS Nano*, 2011, **5**, 6916–6924.
34 A. Fasolino, J. H. Los and M. I. Katsnelson, *Nat. Mater.*, 2007, **6**, 858–861.
35 A. Locatelli, K. R. Knox, D. Cvetko, T. O. Mentes, M. A. Nino, S. C. Wang, M. B. Yilmaz, P. Kim, R. M. Osgood and A. Morgante, *ACS Nano*, 2010, **4**, 4879–4889.
36 S. Plimpton, *J. Comput. Phys.*, 1995, **117**, 1–19.
37 A. J. Schmidt, X. Y. Chen and G. Chen, *Rev. Sci. Instrum.*, 2008, **79**, 114902.
38 B. C. Gundrum, D. G. Cahill and R. S. Averback, *Phys. Rev. B: Condens. Matter Mater. Phys.*, 2005, **72**, 245426.
39 Z. P. Xu and M. J. Buehler, *J. Phys.: Condens. Matter*, 2012, **24**, 475305.
40 J. C. Zhang and X. W. Wang, *Nanoscale*, 2013, **5**, 734–743.